Available online at www.sciencedirect.com

ScienceDirect

Procedia Structural Integrity 2 (2016) 1335–1342

Structural Integrity Procedia

www.elsevier.com/locate/procedia

21st European Conference on Fracture, ECF21, 20-24 June 2016, Catania, Italy

Creep crack propagation behavior in submicron gold films

Hiroyuki Hirakata[a,]*, Ryota Kotoge[a], Takumi Kameyama[a] Toshiyuki Kondo[a], Masayuki Sakihara[a], Kohji Minoshima[a]

[a]*Osaka univesity, Department of Mechanical Engineering, 2-1 Yamadaoka, Suita, Osaka 565-0871, Japan*

Abstract

Creep crack propagation experiments on Au freestanding films of ~240 nm and ~390 nm thickness at room temperature were conducted to clarify the creep crack propagation properties and the thickness effects. In all the experiments, cracks stably propagated and the propagation was accompanied by creep deformation. The crack propagation rate da/dt was not uniquely characterized by the stress intensity factor. The steady-state creep J-integral J_s^* was estimated by an approximate equation using the experimental crack center opening displacement rate. The creep crack propagation rate da/dt vs. J_s^* relations were observed within a narrow band irrespective of the specimen width and applied stress, indicating that J_s^* was the dominant mechanical parameter of the creep crack propagation rate in the Au films. Furthermore, the da/dt–J_s^* relations were close to each other in the ~240 nm and ~390 nm films, suggesting that the creep crack propagation properties of the Au films were insensitive to the film thickness in the thickness range of from ~240 nm to ~390 nm.

Keywords: creep; crack propagation; thin films, size effects, creep J-integaral; gold

1. Introduction

Fracture mechanics is used to characterize the creep crack propagation properties of bulk materials. Many experimental studies have confirmed that the creep J-integral J^* is the mechanical parameter dominating the creep crack propagation rate da/dt under the large-scale creep (LSC) condition (Landes and Begley (1976), Nikbin et al. (1976), Ohji et al. (1976), Taira et al. (1979), Riedel (1989)). The authors have recently conducted creep crack

* Corresponding author. Tel.: +81-6-6879-7241; fax: +81-6-6879-7243.
E-mail address: hirakata@mech.eng.osaka-u.ac.jp

10.1016/j.prostr.2016.06.170

propagation experiments on ~390-nm-thick gold (Au) freestanding films at room temperature (Hirakata et al. (2016)). The results indicated that J^* could characterize $\mathrm{d}a/\mathrm{d}t$ irrespective of the specimen width and applied stress.

The objective of this study is to clarify the effects of film thickness on the creep crack propagation properties of Au submicron films. For this purpose, we performed creep crack propagation experiments on ~240 nm thick Au films and evaluated the creep crack propagation rate. By comparing the experimental results with those of the ~390 nm films, we discuss the thickness effects on the creep crack propagation.

Nomenclature

h	film thickness [nm]
w	specimen width [mm]
a_0	half initial notch length [μm]
a	half crack length [μm]
V	crack center opening displacement [μm]
σ	applied stress [MPa]
ε	strain
$\dot{\varepsilon}_\mathrm{s}$	steady-state strain rate [s^{-1}]
T	temperature [K]
t	time [ks]
$\dot{\varepsilon}_\mathrm{eq}$	equivalent strain rate [s^{-1}]
σ_eq	equivalent stress [MPa]
A	coefficient of steady-state power-law creep [$MPa^{-n}\ s^{-1}$]
n	stress exponent of steady-state power-law creep
t_f	fracture time [ks]
t_tr	transition time [ks]
$\mathrm{d}a/\mathrm{d}t$	creep crack propagation rate [m/s]
K	stress intensity factor [MPa $m^{1/2}$]
E	Young's modulus [GPa]
ν	Poisson's ratio
J^*	creep J-integral [MPa m s^{-1}]
J_s^*	steady-state creep J-integral [MPa m s^{-1}]
$C(n)$	coefficient of approximate equation of creep J-integral
σ_net	net stress [MPa]

2. Experimental methods

The tested materials were Au thin films with thicknesses of approximately ~240 nm (195−260 nm) and ~390 nm (359−420 nm)(Hirakata et al. (2016)) deposited by the radio frequency magnetron sputtering method at a base pressure below 2×10^{-5} Pa and an Argon (Ar) pressure of 1.0 Pa. A sacrificial resin layer with a thickness of ~2 μm was spin-coated on a (100) silicon substrate and then Au films were sputtered on the resin layer through specimen-shaped metal shadow masks (Fig.1). The purity of the Au target was more than 99.9%. The dumbbell-type smooth specimens shown in Fig. 1(a) were used for creep strain rate experiments. The hourglass-type specimens with different widths, w = 2 mm in Fig. 1(b) and w = 1 mm in Fig. 1(c), were utilized for the creep crack propagation experiments to clarify the mechanical parameter dominating the creep crack propagation regardless of specimen size. The hatched regions in the figures represent the fixed parts attached to chucking jigs. The thickness h of each specimen was measured using a stylus surface profiler (KLA-Tencor Japan Ltd., ALPHASTEP500, resolution: 0.1 nm), and the average thickness and standard deviation of 10 measurement sites in each specimen are listed in Table 1. Four specimens were prepared for each thickness film (Specimens 240-1−240-4 for ~240 nm film and Specimens 390-1−390-4 for ~390 nm film). Crystal orientation maps of the film surfaces are shown in Fig. 1(e). A strong {111} preferred surface was observed in all the specimens, and the geometric mean grain sizes were 62 nm for ~240

nm films and 64 nm for ~400 nm films, respectively. A center notch with initial length $2a_0$ (shown in Fig. 1(d)) was introduced in the hourglass specimens using a focused ion beam (FIB) (Hitachi High-Tech Science Corp., SMI9200, or FEI, Versa 3D) system. The half initial notch length a_0 of each specimen is listed in Table 1.

An experimental setup for creep testing of freestanding films previously developed by Hirakata et al. (2012) was used for the experiments. The machine can apply a dead load on a thin film specimen via a weight through a link mechanism, and the elongation of the specimen is measured by a laser displacement sensor (Keyence Corporation LC-2420, range: ±3 mm, resolution: 0.2 μm). The crack length $2a$ and the crack center opening displacement V, defined in Fig. 1(d), were evaluated using a digital optical microscope (HIROX Co., Ltd., KH-2700, magnification: 300x). The applied gross stress σ are listed in Table 1. The experiments were conducted at room temperature in the range 295.3–299.2 K, as listed in Table 1, in laboratory air.

Table 1 Specimen sizes, experimental conditions, and experimental results of creep crack propagation experiments.

Specimen No.	Thickness h, nm	Width w, mm	Half notch length a_0, μm	Applied stress σ, MPa	Testing temperature T, K	Fracture time t_f, ks	Transient time t_{tr}, ks
240-1	260±18	2	49	160	298.9±0.3	40.3	0.84
240-2	212±17		100	120	298.9±0.4	699.3	3.2
240-3	258±13		24	170	298.8±0.4	79.0	0.51
240-4	195±5	1	50	160	299.2±0.5	88.4	0.93
390-1	359±15	2	50	160	296.0±0.6	395.5	4.9
390-2	400±13		97	120	296.6±0.8	1160.7	10.2
390-3	370±10		25	170	296.9±1.0	670.2	4.0
390-4	420±9	1	49	160	295.3±0.1	29.41	5.1

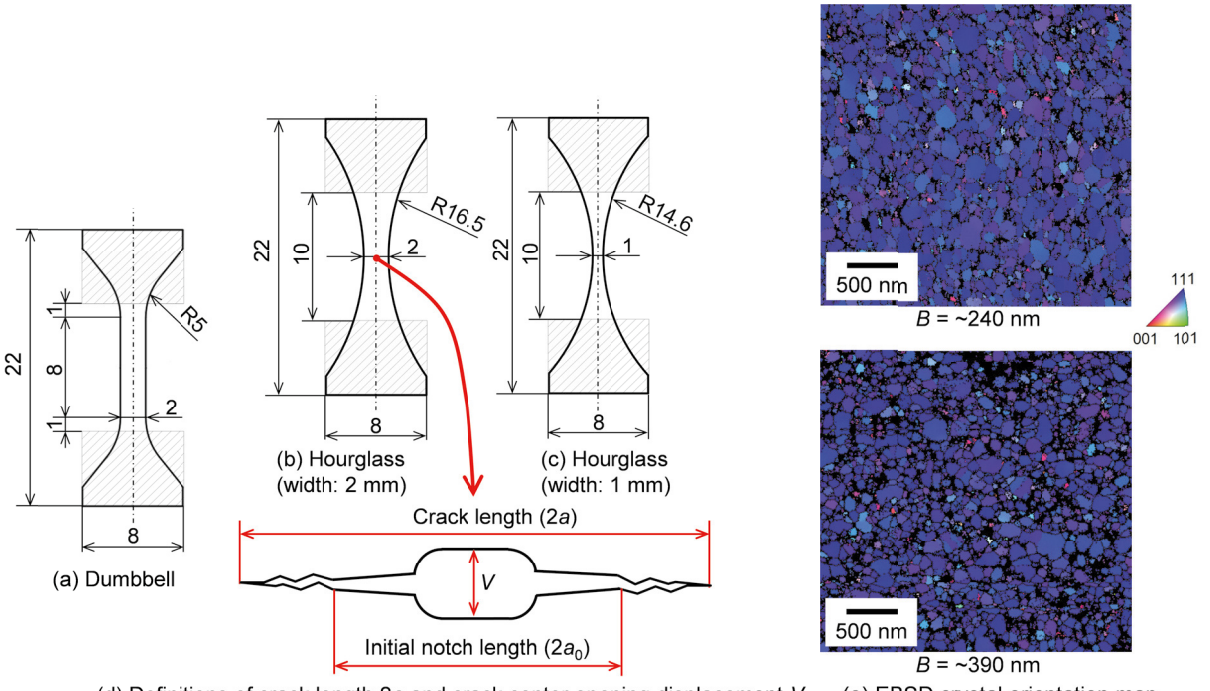

Fig.1 Specimen configurations of Au freestanding films. (a) Dumbbell type specimen is used for creep strain rate experiments. (b) and (c) Hourglass type specimens are used for creep crack propagation experiments. (d) Definitions of crack length and crack center opening displacement. (e) EBSD crystal orientation maps of film surfaces.

3. Results and discussions

3.1. Experimental results

For the smooth specimens, creep experiments were conducted and the results were summarized in Fig.3. The specimens showed creep behavior consisting of transient creep and steady-state creep and then fractured as shown in Fig. 3(a). No clear evidence of an accelerated creep stage was observed. The steady-state creep rate $\dot{\varepsilon}_s$ was estimated from the slope of the steady-state region in the creep curve, as shown by the dashed line in Fig. 3(a). Figure 3(b) shows the relationships between the steady-state strain rate $\dot{\varepsilon}_s$ and the applied stress σ. The creep rate $\dot{\varepsilon}_s$ increased as σ increased and approximately followed the power-law equation in Eq. (1).

$$\dot{\varepsilon}_{eq} = A\sigma_{eq}{}^{n} \qquad (1)$$

Here, $\dot{\varepsilon}_{eq}$ is the von Mises equivalent strain rate, σ_{eq} is the von Mises equivalent stress. The steady-state creep properties A and n were determined by least squares fitting as $A = 9.9\times10^{-21}$ MPa^{-n}s^{-1} and $n = 6.0$ for ~240 nm films and $A = 4.86\times10^{-16}$ MPa^{-n}s^{-1} and $n = 3.6$ for ~390 nm films, respectively. The creep exponent n was close to the value for dislocation creep (n = 3–7).

Figure 4(a)-(c) shows microscope images around the center crack from a creep crack propagation experiment (Specimen 240-1). A wrinkle was observed around the notch and the wrinkled region spread symmetrically in four oblique directions. Because of the wrinkle formation, the crack length measured by microscope images was expected to be shorter than the true crack length. Thus, the crack length was corrected by a method described in the literature (Hirakata et al. (2016)). A crack was initiated at each notch root and propagated in the directions normal to the loading axis. The half crack length a was plotted as a function of t in Fig. 4(d). The cracks stably propagated by t = 40.3 and then unstably fractured. The crack propagation decelerated at first and then gradually accelerated with time. The high crack propagation rate in the very early stage might be due to the large driving force for creep crack propagation under the small-scale creep (SSC) and the transient state from SSC to LSC. The qualitatively similar crack propagation behaviour was observed in the other specimens. The fracture time t_f, which was defined as the time at the unstable fracture, is listed in Table 1.

Figures 5 and 6 show field emission scanning electron microscope (FESEM)(FEI, Versa 3D) micrographs of the fracture surfaces after the creep crack propagation experiments for the ~240 nm specimen (Specimen 240-1) and a ~390 nm specimen (Specimen 390-2, Hirakata et al. (2016)). In both specimens, similar fracture surface morphologies were observed. That is to say, in the region near the notch root (Figs. 5(a) and 6(a)), a chisel point fracture surface was observed locally, and no significant damage was recognized on the film surface. In the early stage of the experiment, the creep crack propagation was expected to be accompanied by creep deformation at the local region under SSC and transient condition as the crack propagation rate was high. In the region where the crack slowly propagated (Fig. 5(b),(c), and Fig. 6(b),(c)), the fracture surface was characterized by fine roughness, which might be due to the microstructure of film, and the observations on the film surfaces revealed that the creep damage was observed on the surface several micrometers away from the crack path. In this region, the crack propagated slowly accompanied by widespread creep deformation around the crack tip.

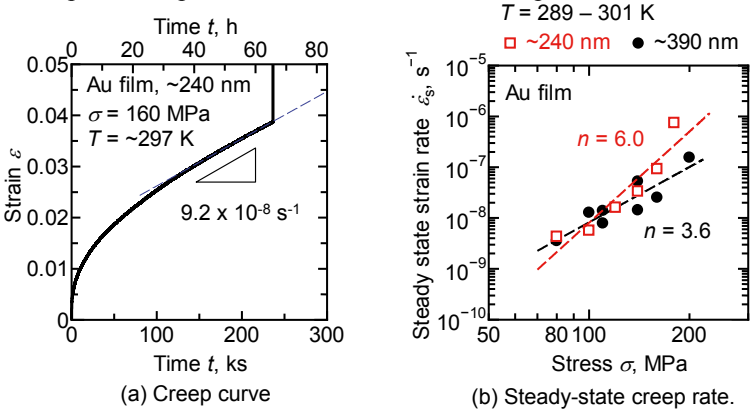

Fig.3 Results of creep experiments for dumbbell type smooth specimens.

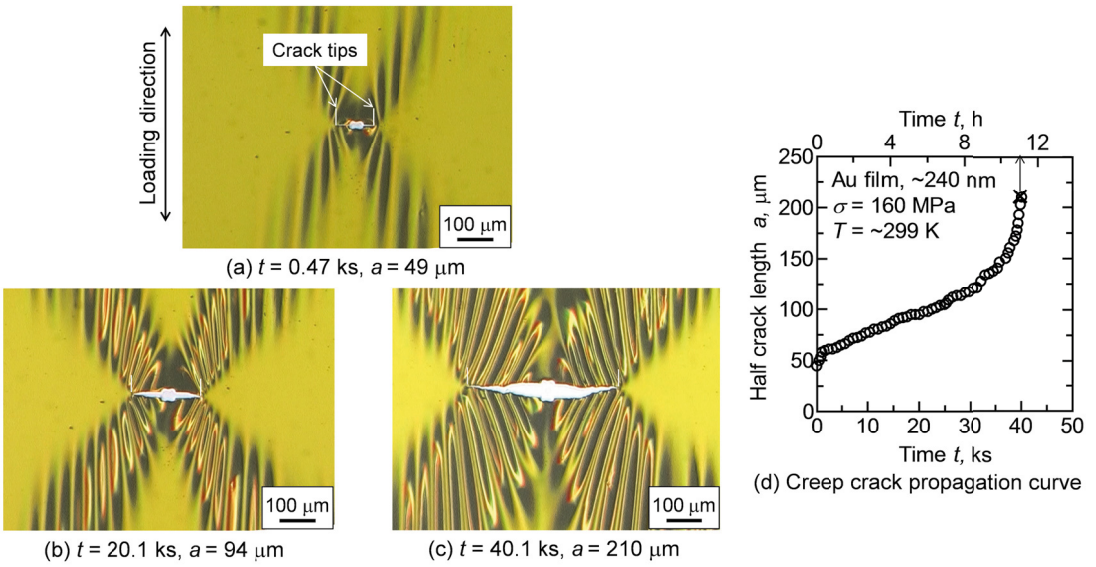

Fig. 4 Results of a creep crack propagation experiment of a 240-nm-thick specimen (Specimen 240-1: $w = 2$ mm, $\sigma = 160$ MPa). (a)-(c) Microscope images. (d) Creep crack propagation curve.

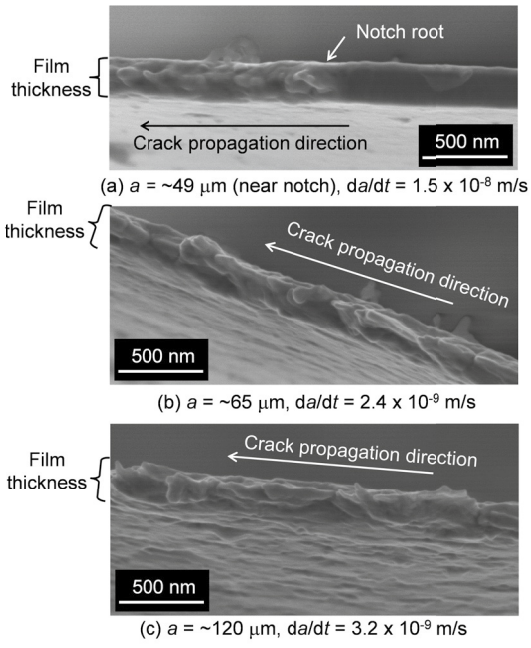

Fig.5 FESEM images of fracture surfaces of a 240-nm-thick specimen (Specimen 240-1).

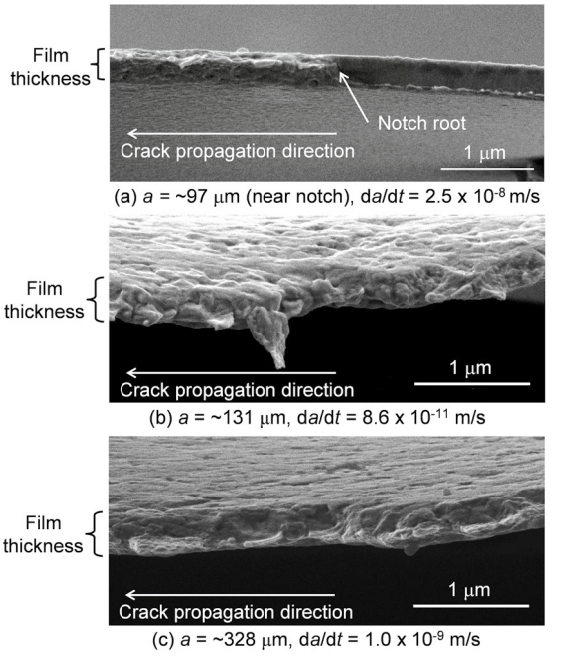

Fig.6 FESEM images of fracture surfaces of a 390-nm-thick specimen (Specimen 390-2) (Hirakata et al. (2016)).

3.2. Discussions

First, we discuss the dominant mechanical parameter that characterizes the creep crack propagation rate. The creep crack propagation rate $\mathrm{d}a/\mathrm{d}t$ was estimated as follows. A quadratic approximation line was obtained by using nine successive points in the a–t relationship (e.g. Fig. 4(d)) around each evaluation point. Then, $\mathrm{d}a/\mathrm{d}t$ was obtained as the derivative of the approximated line at each evaluation point. The stress intensity factor K of the hourglass specimens was calculated by elastic finite element method (FEM) using the commercial code Abaqus 6.13. Figure 7 plots $\mathrm{d}a/\mathrm{d}t$ with respect to K. In all the specimens, $\mathrm{d}a/\mathrm{d}t$ decreased in spite of increasing K in the small-K region. In the large-K region, $\mathrm{d}a/\mathrm{d}t$ increased as K increased. The $\mathrm{d}a/\mathrm{d}t$ – K relations depended on the specimen size and experimental conditions. Thus, K did not uniquely correlate with $\mathrm{d}a/\mathrm{d}t$. This is because the specimen largely deformed by creep around the crack tips in almost the entire crack propagation stage, and hence the use of the elastic stress intensity factor is not valid.

The creep J-integral J^* in the hourglass specimens was estimated under the plane stress condition by FEM. The creep analysis assumed that the Au films obeyed the power-law equation in Eq. (1) and the steady-state creep properties A and n evaluated by the smooth specimens (Fig.3) were used. The Young's modulus E = 80 GPa and Poisson's ratio ν = 0.44 of bulk Au were used. In the power-law creeping material, J^* characterizes the intensity of the HRR singular stress (and strain rate) field (Hutchinson (1968), Rice and Rosengren (1968)). The transition time t_{tr} from SSC to LSC under the plane stress condition is expressed by Eq. (2) (Ohji et al. (1980), and Riedel and Rice (1980)).

$$t_{\mathrm{tr}} = \frac{K^2}{E(n+1)J_s^*} \tag{2}$$

Here, J_s^* is the steady-state creep J-integral, and the values were calculated by the FEM. The transition time t_{tr} obtained by the stationary crack models (Hirakata et al. (2016)) with $a = a_0$ was summarized in Table 2. The transition time t_{tr} was much shorter than the fracture time t_{f} in all the specimens. The $\mathrm{d}a/\mathrm{d}t$ for $t < t_{\mathrm{tr}}$ was plotted with * marks in Fig. 7, and the region of decreasing $\mathrm{d}a/\mathrm{d}t$ roughly corresponded to the transient state region $t < t_{\mathrm{tr}}$. In most of the crack propagation stage, the cracks were expected to propagate under the steady-state or LSC condition. In this case, the steady-state creep J-integral J_s^* characterizes the crack tip mechanical state. In the evaluation of the J-integral by FEM, the error due to the constitutive equation and the material constants A and n becomes large. Therefore, we used an approximate equation for the creep J-integral J^* expressed by Eq. (3) , which was formulated for a long center crack in a rectangular specimen under mode I loading by Ohji et al. (1978).

$$J^* = C(n)\sigma_{\mathrm{net}}\frac{dV}{dt} \tag{3}$$

Here, $C(n)$ is the coefficient depending only on the stress exponent n, e.g., expressed by $C(n) = (n-1)/(n+1)$, σ_{net} is the net stress defined as $\sigma_{\mathrm{net}} = \sigma w/(w-2a)$, and V is the crack center opening displacement. It should be noted that the use of the experimentally measured V reduces the error due to the constitutive equation compared with the computation of J^* by FEM. In this study, $C(n)$ for the hourglass specimens was numerically estimated by FEM, and the $C(n)$ values of ~240 nm and ~390 nm films were 0.95 and 0.69, respectively.

Figure 8 shows the $\mathrm{d}a/\mathrm{d}t$ with respect to the J_s^* calculated by Eq. (3) using the experimental $\mathrm{d}V/\mathrm{d}t$. The experimental $\mathrm{d}V/\mathrm{d}t$ was estimated using the V–t relations evaluated from the microscope images. The $\mathrm{d}a/\mathrm{d}t$–J_s^* relations were observed to be within a narrow band irrespective of the specimen width w and applied stress σ in each thickness film. J_s^* almost uniquely corresponded to $\mathrm{d}a/\mathrm{d}t$, unlike K in Fig. 7. Thus, the results indicated that the creep J-integral J_s^* was the dominant mechanical parameter that characterized the creep crack propagation rate of the Au films. In Fig. 8, the data points in the transient state $t < t_{\mathrm{tr}}$ are shown with * marks. The decrease in the crack propagation rate in the very early stage was due to the decrease in J^* during the transition from SSC to LSC. Although J_s^* from Eq. (3) represents the mechanical state under the steady-state condition, $\mathrm{d}a/\mathrm{d}t$ in the transient stage was roughly within the same narrow band.

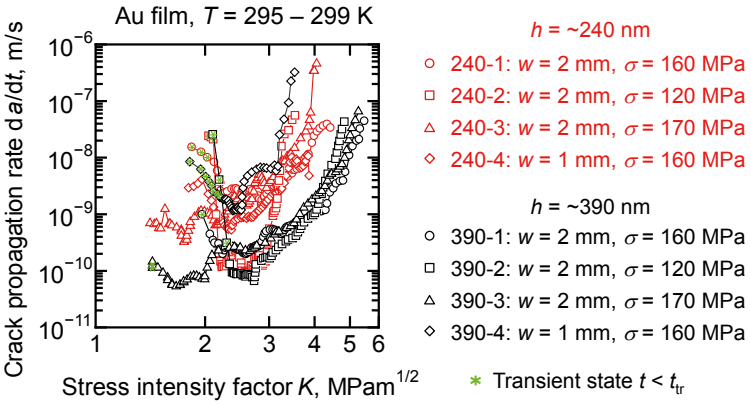

Fig. 7 Relationship between crack propagation rate and stress intensity factor.

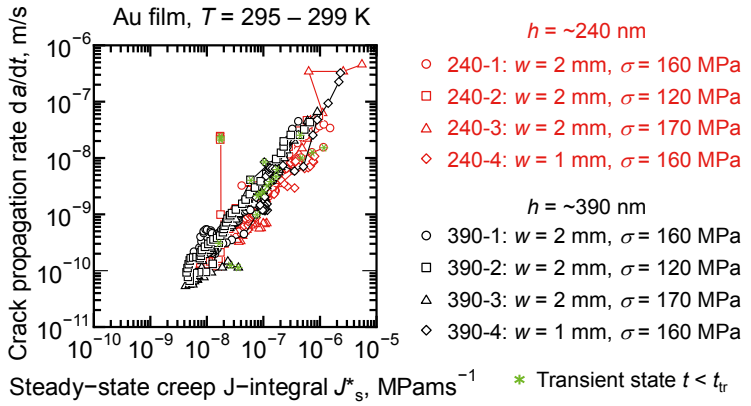

Fig. 8 Relationship between crack propagation rate and steady-state creep J-integral.

Next, we discuss the effect of film thickness on the creep crack propagation properties. The $\mathrm{d}a/\mathrm{d}t$–J_s^* relations were close to each other in the ~240 nm and ~390 nm films, as confirmed in Fig. 8. This suggested that the creep crack propagation properties of Au films were insensitive to the film thickness in the thickness range of from ~240 nm to ~390 nm. However, as the thickness range was very narrow, further studies are needed to investigate the thickness effects in the wider thickness range. In our future plan, we will address the creep crack propagation properties in the thinner and thicker samples and clarify the size effects in the submicron-thickness range.

4. Conclusions

In order to clarify the creep crack propagation properties and the thickness effects of Au submicron films, we conducted creep crack propagation experiments on freestanding ~240 nm and ~390 nm specimens with a center notch at room temperature. The steady-state creep properties, i.e., the coefficient A and the exponent n of the power-law, of the Au films were obtained as $A = 9.9\times10^{-21}$ MPa^{-n}s^{-1} and $n = 6.0$ for ~240 nm films and $A = 4.86\times10^{-16}$ MPa^{-n}s^{-1} and $n = 3.6$ for ~390 nm films, respectively, from the creep experiments on smooth specimens. In the creep crack propagation experiments, a crack began to propagate from the notch root, and stably propagated accompanied by large creep deformation in almost the entire crack propagation stage except in the very early stage. The crack propagation rate decreased once in the very early stage and then increased. The crack propagation rate $\mathrm{d}a/\mathrm{d}t$ was not uniquely characterized by the stress intensity factor K. The cracks in the experiments propagated under the steady-state or the LSC condition in almost the entire crack propagation stage. Thus, the steady-state creep J-integral J_s^* was estimated by an approximate equation using the experimental crack center opening displacement rate $\mathrm{d}V/\mathrm{d}t$,

and the $\mathrm{d}a/\mathrm{d}t$–J_s^* relations were observed within a narrow band regardless of the specimen width and applied stress in each thickness film. The results indicated that the creep J-integral was the dominant mechanical parameter characterizing the creep crack propagation rate of the Au films. The $\mathrm{d}a/\mathrm{d}t$–J_s^* relations were close to each other in the ~240 nm and ~390 nm films. This suggested that the creep crack propagation properties of Au films were insensitive to the film thickness in the thickness range of from ~240 nm to ~390 nm.

Acknowledgements

This work was supported by the Japan Society for the Promotion of Science (JSPS) Grants-in-Aid for Scientific Research (KAKENHI) Grant Number 26220901.

References

Hirakata H., Fukuhara N., Ajioka S., Yonezu A., Sakihara M., Minoshima K., 2012, The Effect of Thickness on the Steady-State Creep Properties of Freestanding Aluminum Nano-Films. Acta Materialia 60, 4438–4447.

Hirakata H., Kameyama T., Kotoge R., Kondo T., Sakihara M., Minoshima K., 2016, Creep Crack Propagation in Gold Submicron Films at Room Temperature. International Journal of Fracture, in press (doi: 10.1007/s10704-016-0104-z).

Hutchinson J.W., 1968, Plastic Stress and Strain Fields at a Crack Tip. Journal of the Mechanics and Physics of Solids 16, 337–342.

Landes J.D., Begley J.A., 1976, A Fracture Mechanics Approach to Creep Crack Growth. ASTM STP 590, 128–148.

Nikbin K.M., Webster G.A., Turner C.E., 1976, Relevance of Nonlinear Fracture Mechanics to Creep Cracking. ASTM STP 601, 47–62.

Ohji K., Ogura K., Kubo S., 1976, Mechanics of Creep Crack Propagation under Longitudinal Shear and Its Applications (in Japanese). Transactions of the Japan Society of Mechanical Engineers 42, 350–358.

Ohji K., Ogura K., Kubo S., 1978, Estimates of J-integral in the General Yielding Range and Its Application to Creep Crack Problems (in Japanese). Transactions of the Japan Society of Mechanical Engineers 44, 1831–1838.

Ohji K., Ogura K., Kubo S., 1980 Stress Field and Modified J-integral near a Crack Tip under Condition of Confined Creep Deformation (in Japanese). Journal of the Society of Materials Science, Japan 29, 465–471.

Rice J.R., Rosengren G.F., 1968, Plane Strain Deformation near a Crack Tip in a Power-Law Hardening Material. Journal of the Mechanics and Physics of Solids 16, 1–12.

Riedel H., 1989, Creep Crack Growth. ASTM STP 1020, 101–126.

Riedel H., Rice J.R., 1980, Tensile Cracks in Creeping Solids. ASTM STP 700, 112–130.

Taira S., Ohtani R., Kitamura T., 1979, Application of J-integral to High-Temperature Crack Propagation: Part I — Creep Crack Propagation. Journal of Engineering Materials and Technology 101, 154–161.